

# Spin noise and Bell inequalities in a non ideal superconductor-dot entangler

Olivier Sauret<sup>a</sup>, Thierry Martin<sup>b</sup>, and Denis Feinberg<sup>a</sup>

<sup>a</sup> Laboratoire d'Etudes des Propriétés Electroniques des Solides,  
CNRS, BP 166, 38042 Grenoble Cedex 9, France

<sup>b</sup> Centre de Physique Théorique, Université de la Méditerranée, Case 907, 13288 Marseille, France

Charge and spin current correlations are analyzed in an electron spin entangler built of a superconductor and two quantum dots in parallel. Parasitic processes and spin flip processes are fully described in a density matrix framework. The way they reduce both the efficiency and the fidelity of the entangler is quantitatively analyzed. The violation of the Bell inequalities, as a test of non-locality (entanglement) of split pairs, is formulated in terms of the correlations of electron charge and spin numbers counted in a specific time window  $\tau$ . The efficiency of the test is analyzed, comparing  $\tau$  to the various time scales in the entangler operation.

PACS numbers: 73.23.Hk, 74.78.Na, 03.65.Ud

Manifestations of entanglement in condensed matter have emerged as a mainstream in nanoelectronics. Indeed, entanglement between electrons could be used for building logical gates and quantum communication devices. As for photons in quantum optics, one may consider nano-devices where electrons are essentially free[1]. Alternatively, exploiting the interaction between electrons allows to use the electron spin as a qbit [2], owing to spin coherence times ranging in semiconductors from fractions of  $\mu s$  (bulk [3]) to fractions of  $ms$  ( $T_1$  in quantum dots [4]). Spin entanglement [5, 6, 7] and teleportation[8] scenarios have been proposed. However, in any device one needs a precise control of unwanted electronic transitions which may spoil entanglement and introduce decoherence. Owing to the key importance of entangled pairs in quantum information, we present in this letter a detailed analysis of such a source.

The entangler of Ref.6 is made from a superconductor (S), adjacent to two small quantum dots connected to two normal leads. The dots filter electrons one by one in a single orbital level, and Cooper pairs emitted from the superconductor are split in the two dots – crossed Andreev process (CA)[9]. Ideally, the constituent electrons then propagate in the two normal leads as an entangled pair. Parasitic processes in the entangler include cotunneling (CT)[9, 10] between the two dots via S, and tunneling of a pair through the same lead (Fig. 1). The main (CA) process and the latter process (but not CT) were studied independently of each other in Ref. 6, using perturbation theory. In the same spirit, Ref. 11 used a beam splitter on the output, in order to detect the entangled singlets [12]. In reality, pairs are mixed to a certain degree and the full electron flow should be instead characterized by its density matrix. The present work is based on a quantum master equation scheme which treats all processes on an equal footing [13] and give access to the full density matrix of emitted electrons. It is used to compute the charge and spin correlations in the current flowing through the two branches of the entangler. In particular, spin current correlations[14], even taken at zero fre-

quency, are shown to quantify the entangler's efficiency and fidelity. Next, the violation of Bell inequalities (BI) can be tested by computing the cross correlators of charge and spin particle numbers in a given time window.

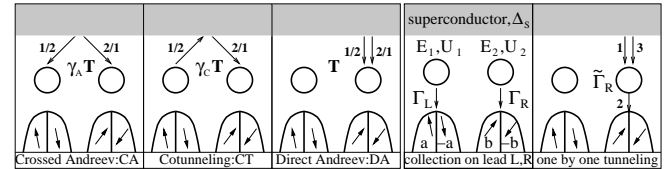


FIG. 1: Processes involved in the operation of the entangler (the order of elementary transitions involving virtual states is indicated) : Crossed Andreev (CA) produce split pairs and triggers entanglement. CT (cotunneling), Direct Andreev (DA) as well as one-by one tunneling through the same dot spoil entanglement. The leads  $L, R$  collect electrons along predefined spin polarizations  $\pm a, \pm b$  (4th panel).

Transport is described by the processes connecting the different states – identified by the charge number and spin of the dots. These include both incoherent processes (transitions between the dots and the leads) and coherent processes (CA, CT and DA, see (Fig. 1)). In the ideal operation of this entangler, the Coulomb blockade prevents double occupancy in each dot. Starting from an empty orbital state (denoted 00), crossed Andreev (CA) reflection couples to a singlet state shared between the two dots,  $11_s$  with an amplitude  $\gamma_A T$  ( $\gamma_A \ll 1$  is the geometrical factor [6, 9, 15]). For a resonant CA transition, the dot energy levels  $E_i$  satisfy  $E_1 + E_2 = 0$ . The two electrons are collected into the leads (whose chemical potentials are  $\mu_{L,R} < E_1, E_2$ ) by transitions to states 01 or 10, then 00, with rates  $\Gamma_i$  ( $i = 1, 2$ ).

If, on the other hand, the intradot Coulomb charging energy  $U$  is not so strong, a coherent transition from 00 to a doubly occupied dot state 20 or 02 can occur via a direct Andreev (DA) process, with a rate  $T$  larger than for CA. Electrons are successively collected by a single lead, with rates  $\Gamma'_i$  then  $\Gamma_i$ , eventually reaching the empty state 00. This transport channel implies dot energies

$2E_i + U$ . In addition, DA can also start from an initial state 10 or 01, proceeding through states 21 (or 12) with energies  $2E_1 + E_2 + U$  ( $E_1 + 2E_2 + U$ ). Further collection into the leads either give states 20 (02), or singlet and triplet states  $11_{s,t}$ , showing that this process is a source of decoherence. In another process, the two electrons from a Cooper pair can tunnel one by one towards the same lead, involving a singly occupied virtual state which costs an energy at least equal to the superconducting gap  $\Delta_S$  (Fig. 1)). Contrary to the DA process, the dot is emptied before the quasiparticle in S is annihilated. The state 10 (01) is reached by an incoherent process with a rate  $\tilde{\Gamma}_i \sim \Gamma_i T_i^2 / \Delta_S^2$ . Last, CT involves a coherent transition of an electron from one dot to the other via S, and mixes all the above processes : it couples states 01 and 10, but also 20 (02) and 11, 21 and 12. CT has an amplitude  $\gamma_C T \ll T$ .

The density matrix equations involving populations (diagonal elements) and coherences (nondiagonal elements) include these processes altogether in a consistent and non-perturbative manner[13]. One can then directly compute the average current, and also the conditional probabilities – for a transition to a given state, assuming a previous initial state – which enter the calculations of the noise correlators [16].

An understanding of the charge and spin correlations can be obtained by considering the spin-resolved zero-frequency noise[14] :  $I_\sigma$  being the current carried by spin  $\sigma$  electrons,  $S_{ij}^{\sigma\sigma'}(0) = \int dt \langle \{\Delta I_i^\sigma(t), \Delta I_j^{\sigma'}(0)\} \rangle$ , where  $i, j = \{L, R\}$  and  $\Delta I_i^\sigma(t)$  is the deviation from average  $\langle I_i^\sigma \rangle = I_i/2$  (assuming spin-symmetric leads). By definition, the total charge/spin current noise reads  $S_{ij}^{ch/sp} = \sum_\sigma (S_{ij}^{\sigma\sigma} \pm S_{ij}^{\sigma-\sigma})$ . The total average current can be written  $I = I_L + I_R$  by denoting the total lead currents by  $I_L = 2I_{LL} + I_{LR}$ ,  $I_R = 2I_{RR} + I_{LR}$ . Here  $I_{LR} = \frac{1}{2}p_S I$ ,  $I_{LL} = \frac{1}{2}p_L I$  and  $I_{RR} = \frac{1}{2}p_R I$  respectively count split pairs and pairs passing through L or R in unit time (with probabilities such that  $p_L + p_R + p_S = 1$ ). It is essential to notice that the spin current fluctuations due to electrons of a given pair are correlated, but those due to different pairs are not, as they pertain to different singlets. This property contrasts with the charge current fluctuations which correlate successive pairs due to Pauli principle. This shows that the spin noise is the right tool to study the spin correlations inside pairs with zero-frequency noise. One can write :

$$\begin{aligned} S_{LL}^{sp} &= 2eI_L - 4eI_{LL}(1 - f_L) = 2eI[p_L f_L + \frac{1}{2}p_S] \\ S_{RR}^{sp} &= 2eI_R - 4eI_{RR}(1 - f_R) = 2eI[p_R f_R + \frac{1}{2}p_S] \\ S_{LR}^{sp} &= S_{RL}^{sp} = -2eI_{LR}(1 - f_S) = -eI p_S (1 - f_S), \quad (1) \end{aligned}$$

and  $S_{tot}^{sp} = 2eI F_S$  is the spin noise of the total current, with  $F_S = p_L f_L + p_R f_R + p_S f_S$  a "spin" Fano factor. Such a factor is equal to zero for maximal spin (anti)correlations, and to one in absence of spin corre-

lations [14]. The first term in  $S_{ii}^{sp}$  corresponds to the autocorrelation of electron wavepackets [14, 16]. The other terms are negative and reflect the spin anticorrelation inside pairs. The Fano-like reduction factors  $f_i, f_S$  quantify this correlation : for instance, blocking one lead ( $\Gamma_R = 0$  for instance), all pairs pass through L ( $p_L = 1$ ) in a sequential way. In this case  $I_L = 2I_{LL}$  and  $f_L = 0$ , i. e. the spin noise through L is zero[14]. On the other hand, if the entangler operates ideally (only CA),  $p_S = 1$ ,  $f_S = 0$  and  $S_{ii}^{sp} = eI$ , while  $S_{LR}^{sp} = -eI$ . In general, pairs are both distributed (through LL, RR and LR) and mixed together : due to states with three electrons in the double dot, two electrons of a split pair L, R can be separated by a time interval during which a few pairs pass through a single dot (as illustrated by the sequence 00, 11, 10, 12, 11, 10, 00). This variable delay between two spin-correlated electrons is responsible for the factors  $f_{L,R,S} > 0$  which measure the degree of mixing.

This suggests that parasitic processes have two effects : i) to reduce the probability of split pairs,  $p_S$  defining the entangler's efficiency and ii) to reduce the spin correlation of a split pair,  $1 - f_S$  defining the fidelity of the entangler, measured here by zero-frequency noise. We now illustrate these trends quantitatively. Charge and spin noise correlations are calculated from the entangler's quantum master equations [13], neglecting four-electron states for simplicity.

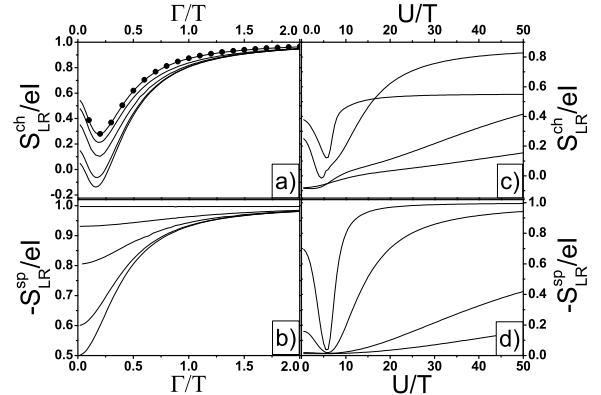


FIG. 2: Spin current cross-correlations, assuming CA to be resonant:  $E_1 + E_2 = 0$ , and  $\Gamma_L = \Gamma_R$ .  $\Delta_S$  is the largest energy scale, thus one-by-one tunneling is negligible. In a) and b), only CA and CT are taken into account, assuming  $U \rightarrow \infty$ . Charge and spin cross-correlations are plotted for  $0 < \Gamma < 2$  and several values of  $E = |E_1 - E_2| = \{0, 0.2, 0.5, 1, 5\}$ . The dotted line is the ideal case. c) and d) correspond to  $0 < U < 50$  and  $E = 5$  (no CT), for  $\Gamma_{L,R} = \{0.01, 1, 5, 10\}$  (top to bottom).

Consider the ideal operation (CA only) for different  $\Gamma$ 's (assuming  $T = 1$ ). Then all electron pairs are split and cross the device sequentially. The average current  $I$  [13]

(Fig. 4a) displays a maximum in the region  $\Gamma \sim \gamma_A T$ , in a way analogous to the current through a single dot where in/out transition rates  $\Gamma_{in}$ ,  $\Gamma_{out}$  are equilibrated in a sequential regime. The crossed charge noise  $S_{LR}^{ch}$  is positive (Fig. 2a), in contrast to the partition noise of single electrons. This reflects the perfect charge correlation of split pairs [17].  $S_{LR}^{ch}$  displays a minimum (Fig. 2a) and becomes Poissonian only in the limit  $\Gamma \gg \gamma_A T$ , where successive pairs do not correlate. Notice that in the ideal operation one has  $S_{LR}^{ch} = S_{LL}^{ch} = S_{RR}^{ch}$ . On the other hand, one checks that  $S_{ii}^{sp} = -S_{LR}^{sp} = eI$ .

Parasitic processes are next illustrated in presence of CT alone ( $U$  and  $\Delta_S$  infinite). Pairs are then distributed ( $LL$ ,  $RR$  and  $LR$ ) but still sequential (they do not mix): all the  $f$ 's in Eq. (1) are equal to zero.  $S_{LR}^{ch}$  decreases (Fig. 2a) and can even become negative, e. g. partition noise dominates over pair correlations. On the other hand, spin noise  $S_{ii}^{sp} = -S_{LR}^{sp} = eIp_s$ , the spin Fano factor simply counting the split pairs (Fig. 2b). One checks that the total spin noise  $S_{LL}^{sp} + S_{RR}^{sp} + 2S_{LR}^{sp}$  is zero, i. e. the whole entangler is a perfect Andreev source. Notice that  $p_s$  tends to one for large  $\Gamma \gg \gamma_C T$  where CT has no time to occur. Moreover, for large  $|E_1 - E_2|/T > 5$ , CT is merely suppressed.

Next, double occupancy in the dots is allowed. Fixing  $\Gamma/T$ , the crossed charge noise is reduced and can become negative at small  $U$  (Fig. 2c). Spin noise correlations decrease as  $U/T$  decreases (Fig. 2d). For small  $\Gamma$ , the probability to have split Cooper pairs displays a minimum, due to resonant DA transitions when  $E_i \sim -U$ . The width of this minimum increases for large  $\Gamma$ , due to two competing processes. On one hand, the probability for having a split pair (CA) in the 2 dots oscillates on a time scale  $(\gamma_A T)^{-1}$ , on the other hand, the probability for a DA processes is smaller, but it oscillates more rapidly  $((U^2 + 4T^2)^{-1/2})$  [13]. A larger detection rate thus favors the latter process. In the resonant regime  $S_{LL}^{ch}$  can even approach  $4eI_L$ , e.g. the noise doubling of a NS junction [18]. This analysis demonstrates that optimal pair correlations are obtained if  $\gamma_A T < \Gamma < U$ .

Entanglement should be probed by a BI test. It relies on the measurement [19] of number correlators. One may simplify the response of the electronic circuit such as to measure, not the instantaneous current, but instead the particle number accumulated during a time  $\tau$ ,  $N_\alpha(t, \tau) = \int_t^{t+\tau} dt' I_\alpha(t')$  ( $\alpha = \pm a, \pm b$  see Fig. 1). The inequality which is derived assuming a product density matrix weighted by local hidden variable reads [20]:

$$|G(\mathbf{a}, \mathbf{b}) - G(\mathbf{a}, \mathbf{b}') + G(\mathbf{a}', \mathbf{b}) + G(\mathbf{a}', \mathbf{b}')| \leq 2, \quad (2a)$$

$$G(\mathbf{a}, \mathbf{b}) = \frac{\langle (N_a(\tau) - N_{-a}(\tau))(N_b(\tau) - N_{-b}(\tau)) \rangle}{\langle (N_a(\tau) + N_{-a}(\tau))(N_b(\tau) + N_{-b}(\tau)) \rangle} \quad (2b)$$

In Ref. 20, the correlators  $\langle N_\alpha(\tau)N_\beta(\tau) \rangle$  were related to zero-frequency current noise correlators via an approximate relation. We follow Ref. 21 and calculate

the correlators from first principles. The cross correlator for arbitrary spin directions of the filters can be separated into a parallel and an antiparallel component:  $\langle N_\alpha(\tau)N_\beta(\tau) \rangle = \langle N_{L\uparrow}(\tau)N_{R\downarrow}(\tau) \rangle \sin^2(\theta_{\alpha\beta}/2) + \langle N_{L\uparrow}(\tau)N_{R\uparrow}(\tau) \rangle \cos^2(\theta_{\alpha\beta}/2)$ , with  $\theta_{\alpha\beta}$  the relative angle between the polarizations in  $L$  and  $R$ . With the same choice of angles as considered in Ref. 20 the BI becomes:

$$|\Delta N_{LR}^{sp}/(\Delta N_{LR}^{ch} + \Lambda^+)| \leq 1/\sqrt{2} \quad (3)$$

with  $\Delta N_{LR}^{sp} = \langle N_{L\uparrow}(\tau)N_{R\downarrow}(\tau) \rangle - \langle N_{L\uparrow}(\tau)N_{R\uparrow}(\tau) \rangle$  and  $\Delta N_{LR}^{ch} + \Lambda^+ = \langle N_{L\uparrow}(\tau)N_{R\downarrow}(\tau) \rangle + \langle N_{L\uparrow}(\tau)N_{R\uparrow}(\tau) \rangle$ , where  $\Lambda^+ = \tau^2 \langle I_L \rangle \langle I_R \rangle$  is the reducible part of the charge correlator.

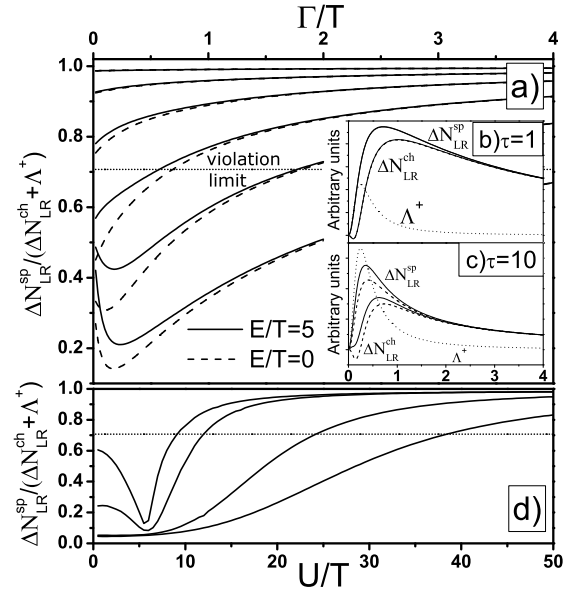


FIG. 3: The left part of the BI is compared to the limit  $2^{-1/2}$ . a) plotted for  $0 < \Gamma_{L,R} < 4$ , two values of  $E$  (0, and 5 which simulates ideal working regime), and  $\tau = \{1, 2.5, 5, 10, 20, 50\}$  (from the top to the bottom). To characterize the BI test, each contribution of  $|\Delta N_{LR}^{sp}|/(\Delta N_{LR}^{ch} + \Lambda^+)$  is plotted for  $\tau = 1$  b),  $\tau = 10$  c). d) Double occupancy is taken into account, assuming  $E_1 = -E_2 = 5$ , and  $\Gamma_{L,R} = \{0.01, 1, 5, 10, 100\}$  (top to bottom) and  $\tau = 1$

In the ideal case (see Fig. 3a), the BI violation is maximal for  $\tau < h/T$ . Increasing  $\tau$ , thus the number of measured pairs, quantum spin correlations show a minimum at  $\Gamma \sim \gamma_A T$ , due to a decrease of  $\Delta N_{12}^{sp/ch}/\Lambda^+$  (Fig. 3b,c). Violation is recovered provided  $\Delta N_{12}^{ch} \sim \tau I$  dominates over  $\Lambda^+ = \tau^2 I^2$ , where  $I \sim \gamma_A^2 T^2/\Gamma$  for large  $\Gamma$  and  $I \sim \Gamma$  for small  $\Gamma$ . This means that pairs should be measured roughly one by one [20]. Now, considering parasitic processes, CT tends to prevent BI violation at small  $\Gamma$ , and for large enough  $\tau$  (Fig. 3a). Finite  $U$  sensibly decreases the quantum spin correlations (Fig. 3d).

Yet, comparing Figs. 2 and 3, one sees that the BI test is much less sensitive than the spin noise to parasitic processes. For instance, with  $\Gamma = 5$  and  $U/T = 40$ , the spin noise is about 0.3 (low efficiency), while the BI is violated with  $\tau = 1$ . In fact, this window allows filtering of split CA pairs, mostly dropping "wrong" DA pairs. Therefore, tuning  $\tau$  to an optimum value yields high fidelity of entanglement, even if the efficiency of the entangler is low.

Finally, the effect spin-flip scattering in the dots is addressed (time scale  $\tau_{sf}$ ). This acts as a decoherence source, due to the transitions of singlet states  $11_s$  towards triplet states. Spin-flip is easily incorporated into the general density matrix equations. Its effect is summarized on Fig. 4. First, the average current is strongly quenched as soon as the spin-flip rate is of the order of the CA amplitude (Fig. 4a). Indeed, such spin-flip suppresses the pair resonance between states  $00$  and  $11_s$  and has an effect similar to decay towards  $L, R$ . For  $\tau_{sf} < h/\Gamma < h/\gamma_A T$ , the current behaves as  $\tau_{sf}^2$ . Spin-flip also decreases charge correlations (Fig. 4b). Second, spin-flip decreases the spin noise correlations in leads  $L, R$  (Fig. 4b), by essentially decreasing the fidelity  $1 - f_s$ . In addition, Bell correlations are also affected by spin-flip, but, as above, much less than spin noise.

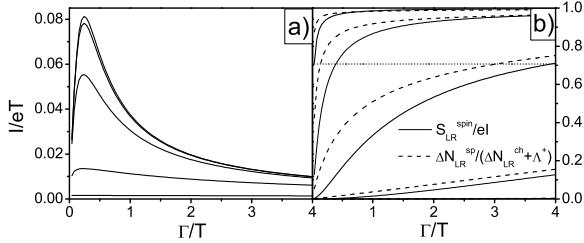


FIG. 4: (a) Average current  $I$ ; (b) spin current noise (continuous) and Bell correlation (dotted), as a function of  $\Gamma/T$ , with  $U = E =$  and finite spin-flip time  $\tau_{sf}$  in the dots.  $\tau_{sf} = 10, 1, 0.1, 0.01$  decreases from top to bottom (same normalization as before).

To summarize, we have shown that zero frequency charge and spin current correlations allow a detailed analysis of the efficiency and fidelity of the entangler in terms of parasitic and spin flip processes. As a result, a satisfactory operation is upon reach with realistic parameters. For injection/detection rates  $T \sim \Gamma \sim 0.1K$ , the shortest time window described in this work corresponds to  $\tau \sim 0.1ns$ , a time scale which is accessible with current fast electronics apparatus. Much longer time scales can be achieved using a weaker coupling to the reservoirs [4].

LEPES is under convention with Université Joseph Fourier. Support from Ministry of Research A.C.

Nanosciences" is gratefully acknowledged.

- [1] C. W. J. Beenakker, C. Emery, M. Kindermann and J. L. van Velsen, Phys. Rev. Lett **91**, 147901 (2003); C. W. J. Beenakker and M. Kindermann, Phys. Rev. Lett **92**, 056801 (2004); P. Samuelsson, E. V. Sukhorukov and M. Büttiker, Phys. Rev. Lett **91**, 157002 (2003); P. Samuelsson, E.V. Sukhorukov, M. Büttiker Phys. Rev. Lett. **92**, 026805 (2004).
- [2] D. Loss and D. P. DiVincenzo, Phys. Rev. A **57**, 120 (1998).
- [3] J. M. Kikkawa and D. D. Awschalom, Phys. Rev. Lett. **80**, 4313 (1998).
- [4] J. M. Elzerman, R. Hanson, L. H. W. van Beveren, B. Witkamp, L. M. K. Vandersypen and L. P. Kouwenhoven, Nature **430**, 431 (2004).
- [5] G. B. Lesovik, T. Martin, and G. Blatter, Eur. Phys. J. B **24**, 287 (2001).
- [6] P. Recher, E. V. Sukhorukov, and D. Loss, Phys. Rev. B **63**, 165314 (2001).
- [7] W. D. Oliver, F. Yamaguchi, and Y. Yamamoto, Phys. Rev. Lett. **88**, 037901 (2002). D. S. Saraga, D. Loss, Phys. Rev. Lett. **90**, 166803 (2003).
- [8] O. Sauret, D. Feinberg and T. Martin, Eur. Phys. J. B **32**, 545 (2003); O. Sauret, D. Feinberg and T. Martin, Phys. Rev. B **69**, 035332 (2004).
- [9] G. Deutscher and D. Feinberg, Appl. Phys. Lett. **76**, 487 (2000); G. Falci, D. Feinberg, and F. W. J. Hekking, Europhys. Lett. **54**, 255 (2001); D. Feinberg, Eur. Phys. J.B **36**, 419 (2003).
- [10] D. V. Averin and Yu. V. Nazarov, in *Single Charge Tunneling*, H. Grabert and M.H. Devoret eds. (Plenum, New York 1992).
- [11] P. Samuelsson, E.V. Sukhorukov and M. Büttiker Phys. Rev. B **70**, 115330 (2004).
- [12] G. Burkard, D. Loss, and E. V. Sukhorukov Phys. Rev. B **61**, R16303-R16306 (2000). G. Burkard and D. Loss Phys. Rev. Lett. **91**, 087903 (2003).
- [13] O. Sauret, D. Feinberg and T. Martin, cond-mat/0402416, Phys. Rev. B (2004, in press); O. Sauret, PhD Thesis (2004).
- [14] O. Sauret and D. Feinberg, Phys. Rev. Lett. **92**, 106601 (2004).
- [15] M. S. Choi, C. Bruder and D. Loss, Phys. Rev. B **62**, 13569 (2000).
- [16] A. N. Korotkov Phys. Rev. B **49**, 10381-10392 (1994)
- [17] J. Torrès and T. Martin, Eur. Phys. J. B **12**, 399 (1999).
- [18] V. A. Khlus, Zh. Éksp. Teor. Fiz. **93**, 2179 (1987) [Sov. Phys. JETP **66**, 1243 (1987)]; X. Jehl, P. Payet-Burin, C. Baraduc, R. Calemczuk and M. Sanquer, Phys. Rev. Lett. **83**, 1660 (1999).
- [19] A. Aspect, J. Dalibard, and G. Roger, Phys. Rev. Lett. **49**, 1804 (1982); A. Zeilinger, Rev. Mod. Phys. **71**, S288 (1999).
- [20] N. M. Chtchelkatchev, G. Blatter, G. B. Lesovik and T. Martin, Phys. Rev. B **66**, 161320(R) (2002).
- [21] A.V. Lebedev, G.B. Lesovik and G. Blatter, cond-mat/0311423.